THE ASTROPHYSICAL JOURNAL, 599:806–813, 2003 December 20

STOCHASTIC GRAVITATIONAL WAVE BACKGROUND: UPPER LIMITS IN THE 10^{-6} TO 10^{-3} Hz BAND

J. W. ARMSTRONG,[1] L. IESS,[2] P. TORTORA,[3] AND B. BERTOTTI[4]

Received 2003 May 25; accepted 2003 September 2

ABSTRACT

We have used precision Doppler tracking of the *Cassini* spacecraft during its 2001–2002 solar opposition to derive improved observational limits to an isotropic background of low-frequency gravitational waves. Using the *Cassini* multilink radio system and an advanced tropospheric calibration system, the effects of heretofore leading noises—plasma and tropospheric scintillation—were, respectively, removed and calibrated to levels lower than other noises. The resulting data were used to construct upper limits to the strength of an isotropic background in the 10^{-6} to 10^{-3} Hz band. Our results are summarized as limits on the strain spectrum $S_h(f)$, the characteristic strain (h_c = the square root of the product of the frequency and the one-sided spectrum of strain at that frequency), and the energy density (Ω = energy density in bandwidth equal to center frequency assuming a locally white energy density spectrum, divided by the critical density). Our best limits are $S_h(f) < 6 \times 10^{-27}$ Hz^{-1} at several frequencies in the millihertz band, $h_c < 2 \times 10^{-15}$ at about 0.3 mHz, and $\Omega < 0.025 \times h_{75}^{-2}$, where h_{75} is the Hubble constant in units of 75 km s^{-1} Mpc^{-1}, at 1.2×10^{-6} Hz. These are the best observational limits in the low-frequency band, the bound on Ω, for example, being about 3 orders of magnitude better than previous constraints from Doppler tracking.

Subject headings: cosmology: observations — gravitational waves — relativity

1. INTRODUCTION

Spacecraft Doppler tracking can be used to detect or constrain the level of low-frequency[5] gravitational waves (GWs). The underlying principle of the detector is that Earth and a distant spacecraft act as separated test masses. An almost monochromatic microwave signal (nominal radio frequency f_0) is transmitted from the ground, phase-coherently transponded at the spacecraft, and received on the ground. By comparing the frequencies of the transmitted and received signals, the Doppler tracking system measures the relative dimensionless velocity $\Delta f/f_0 = 2\Delta v/c$ between Earth and the spacecraft. A gravitational wave having strain amplitude h and characteristic frequency $\sim 1/$(two-way light-time to spacecraft) or larger incident on the Earth-spacecraft system causes Doppler perturbations of order h replicated three times in the time series of $\Delta f/f_0$ (Estabrook & Wahlquist 1975; Wahlquist 1987). The sum of these three perturbations in the Doppler record is zero. In the limit where the characteristic period of the GW signal is $\gg T_2$, where T_2 is the two-way light-time between the spacecraft and Earth, these three events in the Doppler time series overlap and the GW signal contribution in the Doppler record is suppressed. The mean-square low-frequency coupling in this limit is proportional to (Fourier frequency)^2, giving reduced but nonnegligible signal contribution at low frequencies. In this paper we use high-precision Doppler tracking data of the *Cassini* spacecraft to put improved observational upper limits on a stochastic background of gravitational waves in the band 10^{-6} to 10^{-3} Hz.

2. SPACECRAFT DOPPLER TRACKING

The theory of spacecraft Doppler tracking as a GW detector has been developed by Estabrook & Wahlquist (1975) and Wahlquist (1987). Briefly, the gravitational wave response of a coherent two-way Doppler time series of fractional frequency fluctuation $y_2^{\rm gw}(t)$ excited by a transverse, traceless plane gravitational wave having unit wavevector $\hat{k}$ is

$$y_2^{\rm gw}(t) = -\frac{(1-\mu)}{2}\bar{\Psi}(t) - \mu\bar{\Psi}\left[t - \frac{(1+\mu)}{2}T_2\right] + \frac{(1+\mu)}{2}\bar{\Psi}(t-T_2)\,, \quad (1)$$

where $\mu = \hat{k}\cdot\hat{n}$, $\hat{n}$ is a unit vector from Earth to the spacecraft, T_2 is the two-way light-time from Earth to the spacecraft and back, $\bar{\Psi}(t) = [\hat{n}\cdot\boldsymbol{h}(t)\cdot\hat{n}]/[1-(\hat{k}\cdot\hat{n})^2]$, and $\boldsymbol{h}(t)$ is the first-order metric perturbation. The gravitational wave $\boldsymbol{h}(t)$ is $[h_+(t)\boldsymbol{e}_+ + h_\times(t)\boldsymbol{e}_\times]$, where the 3-tensors $\boldsymbol{e}_+$ and $\boldsymbol{e}_\times$ are transverse to $\hat{k}$ and traceless. (We distinguish $\bar{\Psi}$ from the Ψ used in the analysis of the Laser Interferometer Space Antenna [LISA] detector [Armstrong, Estabrook, & Tinto 1999]: $\Psi = \frac{1}{2}\bar{\Psi}$.)

For an isotropic GW background, the sky- and polarization-averaged signal contribution to the spectrum of two-way fractional Doppler fluctuations, $S_{y2}^{\rm gw}(f)$, is

[1] Jet Propulsion Laboratory, California Institute of Technology, Pasadena, CA 91109.

[2] Dipartimento di Ingegneria Aerospaziale e Astronautica, Università di Roma "La Sapienza," 00184 Rome, Italy.

[3] II Facoltà di Ingegneria, Università di Bologna, 47100, Forlì, Italy.

[4] Dipartimento di Fisica Nucleare e Teorica, Università di Pavia, 27100 Pavia, Italy.

[5] Gravitational wave bands divide mostly on detector technology (Thorne 1987). Extremely low frequency ($\sim 10^{-18}$ to $\sim 10^{-15}$ Hz) search programs are based on mapping the intensity and polarization of the cosmic microwave background. Very-low frequency observations ($\sim 10^{-8}$ to $\sim 10^{-5}$ Hz) mostly use pulsar timing observations. Low-frequency observations ($\sim 10^{-6}$ to $\sim 10^{-1}$ Hz) use Doppler tracking of spacecraft or, in the future, laser interferometers in space. High-frequency observations (~ 1 to $\sim 10^4$ Hz) involve ground-based laser interferometers or resonant bar detectors.

related to the spectrum of the gravitational waves, $S_h(f)$, by $S_{y2}^{\rm gw}(f) = \bar{R}_2(f) S_h(f)$, where (Estabrook & Wahlquist 1975)

$$\bar{R}_2(f) = \frac{(\pi f T_2)^2 - 3}{(\pi f T_2)^2} - \frac{\cos(2\pi f T_2)[(\pi f T_2)^2 + 3]}{3(\pi f T_2)^2} + \frac{2\sin(2\pi f T_2)}{(\pi f T_2)^3}. \quad (2)$$

(If a background is not isotropic, then the spectral response function is the square of the Fourier transform of the three-pulse response [eq. (1)], evaluated for the relevant μ and averaged over polarization states; see Armstrong, Estabrook, & Tinto 1999 and Estabrook et al. 2000.) $\bar{R}_2$ shows that GWs couple best to the Doppler at Fourier frequencies larger than or comparable to the reciprocal of the two-way light-time between Earth and the spacecraft. At low frequencies the Earth-spacecraft system is in the long-wavelength limit (LWL); expansion of the response shows suppressed coupling of GWs to the Doppler, $\bar{R}_2(f) \simeq (8/15)(\pi f T_2)^2$ if $(\pi f T_2) \ll 1$.

Gravitational wave signals compete with noises in the Doppler time series. Analysis of noise in Doppler observations, for the band of best GW coupling ($f > T_2^{-1}$), has been done, e.g., by Wahlquist et al. (1977) and Iess et al. (1999). Detailed error budgets for the particular case of *Cassini* are given by Tinto (2002) and Abbate et al. (2003). After best estimates of all deterministic effects (e.g., orbital signature) are removed, the main sources of variability in y_2 are, for $f > 10^{-4}$ Hz, noise due to instability in the frequency standard driving the Doppler system (frequency and timing system [FTS] noise, $y^{\rm FTS}$); phase scintillation due to propagation through the solar wind ($y^{\rm sw}$), ionosphere ($y^{\rm ion}$), and neutral atmosphere ($y^{\rm tropo}$); thermal noise in the receiver due to finite signal-to-noise ratio on the downlink ($y^{\rm rcvr}$); unmodeled motion of the spacecraft ($y^{\rm s/c\,motion}$); mechanical motion of the ground antenna ($y^{\rm ant}$); spacecraft transponder noise ($y^{\rm s/c\,elect.}$); ground electronics noise ($y^{\rm ground\,elect.}$); and systematic errors ($y^{\rm systematic}$). The noises enter with specific transfer functions (Estabrook & Wahlquist 1975; Wahlquist et al. 1977). With the notation that $y_2^{\rm raw}$ is the raw two-way fractional Doppler and an asterisk indicating convolution, the time series can be modeled as

$$\begin{aligned} y_2^{\rm raw}(t) = {} & y_2^{\rm gw} + y^{\rm FTS}(t) * [\delta(t) - \delta(t - T_2)] \\ & + y^{\rm sw}(t) * [\delta(t) + \delta(t - T_2 + 2x/c)] \\ & + y^{\rm ion} * [\delta(t) + \delta(t - T_2)] \\ & + y^{\rm s/c\,elect.}(t) * \delta(t - T_2/2) \\ & + y^{\rm s/c\,motion} * \delta(t - T_2/2) \\ & + y^{\rm ant}(t) * [\delta(t) + \delta(t - T_2)] \\ & + y^{\rm tropo}(t) * [\delta(t) + \delta(t - T_2)] \\ & + y^{\rm ground\,elect.}(t) + y^{\rm rcvr} + y^{\rm systematic}(t)\,, \end{aligned} \quad (3)$$

where x is the effective distance of the solar wind perturbation from Earth. Calibrations to the time series are discussed in the next section. After multilink plasma calibration, phase scintillation due to charged particles is effectively removed. Water vapor radiometer based tropospheric calibration removes $\simeq$90% of the fluctuations due to the neutral atmosphere, so that the calibrated time series, y_2, is approximately

$$\begin{aligned} y_2(t) \simeq {} & y_2^{\rm gw} + y^{\rm FTS}(t) * [\delta(t) - \delta(t - T_2)] \\ & + y^{\rm s/c\,elect.}(t) * \delta(t - T_2/2) + y^{\rm s/c\,motion} * \delta(t - T_2/2) \\ & + y^{\rm ant}(t) * [\delta(t) + \delta(t - T_2)] \\ & + y^{\rm tropo}(t)/10 * [\delta(t) + \delta(t - T_2)] \\ & + y^{\rm ground\,elect.}(t) + y^{\rm rcvr} + y^{\rm systematic}(t) \\ = {} & y_2^{\rm gw} + y_2^{\rm other}(t), \end{aligned} \quad (4)$$

where $y_2^{\rm other}(t)$ is all the non-GW (noise) contribution to the two-way Doppler variability. In the next section we estimate the spectrum of y_2, $S_{y2}(f)$, and discuss the extent to which it can be explained from independent measurements of known noise processes in equation (4). We then use S_{y2} and the GW transfer function (eq. [2]) to determine upper limits to the strength of a GW background in the low-frequency band.

3. OBSERVATIONS AND ANALYSIS

The *Cassini* spacecraft was launched on a mission to Saturn in 1997. After Earth, Venus, and Jupiter gravity assists, it has continued on a free interplanetary cruise trajectory toward orbit insertion at Saturn (mid-2004). The *Cassini* gravitational wave experiment consists of three, 40 day data-taking intervals, centered on the spacecraft's solar oppositions during the 2001–2004 cruise period. The data reported here were taken between 2001 November 26 and 2002 January 4. During that observation interval *Cassini*'s right ascension varied between $05^{\rm h}46^{\rm m}$ and $05^{\rm h}24^{\rm m}$ and its declination between $+22^\circ45'$ and $+22^\circ32'$. The two-way light-time, T_2, between Earth and *Cassini* was about 5730 s at solar opposition (variable over 5710–5880 s during the observations).

The *Cassini* data are distinguished from previous Doppler-tracking GW observations in two ways. First, *Cassini* has a sophisticated multilink radio system that simultaneously allows reception of two uplink signals (at frequencies of X and Ka bands) and transmission of three downlink signals (X-band coherent with the X-band uplink, Ka-band coherent with the X-band uplink, and Ka-band coherent with the Ka-band uplink). (X band, a standard deep space communications frequency, is about 8.4 GHz; Ka band is about 32 GHz.) The two-way Ka-band capability is new and uses a frequency translator provided by the Italian Space Agency to allow reception and phase-coherent retransmission of this signal. The US National Aeronautics and Space Administration (NASA) upgraded one of the Deep Space Network's (DSN) tracking antennas, DSS25 near Goldstone, California, to allow simultaneous transmit/receive capability at X and Ka bands. In the observations reported here, a linear combination of the Doppler data in the multiple links was used to cancel, essentially exactly, plasma phase scintillation (Iess et al. 1999, 2003; Tortora et al. 2002, 2003). Second, DSS25 was also instrumented with a water vapor radiometer based tropospheric phase scintillation calibration system (Resch et al. 2002; Tanner & Riley 2003). This Advanced Media Calibration (AMC) system allowed removal of $\simeq$90% of the Doppler fluctuations caused by radiowave scintillation in the neutral

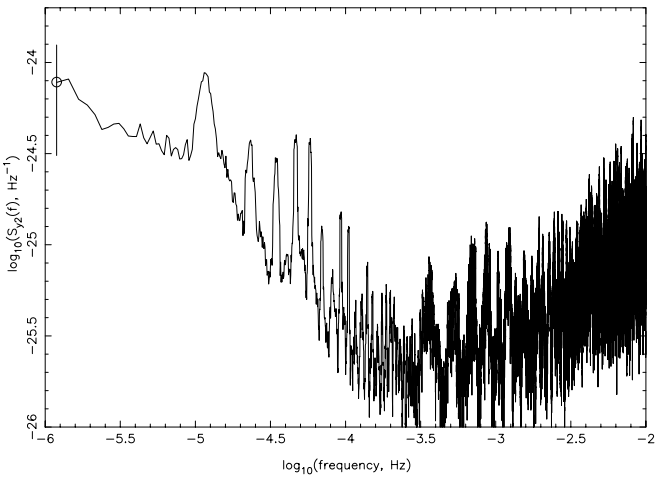

FIG. 1.—Power spectrum of the two-way fractional frequency fluctuations (calibrated for plasma and troposphere) for 2001–2002 *Cassini* solar opposition observations. The spectrum is two-sided and has been smoothed from the intrinsic resolution of the observations to a bandwidth of $\simeq 3$ μHz to reduce estimation error. Representative formal ± 2 σ confidence limits are indicated.

atmosphere. These two instrumental upgrades significantly improve the sensitivities of the gravitational wave search and other *Cassini* radio science investigations (Kliore et al. 2003).

Figure 1 shows the two-sided power spectrum of two-way fractional Doppler frequency, $S_{y2}(f)$, computed from data taken at DSS25 only during the 2001–2002 solar opposition. It is derived from y_2, i.e., after using the multilink plasma corrections and the AMC tropospheric calibrations. Residuals were determined after removal of the orbital Doppler shift using the Orbit Determination Program. (In the postprocessing we also removed a residual line at the frequency of the principal lunar tide, $f = 0.08052$ cycles hr^{-1}, prior to spectral analysis. This corrected an apparent minor misestimation of the lunar Earth tide during orbit removal. The magnitude of the line removed was $\Delta f/f = 6.5 \times 10^{-15}$ at $f = 2.2367 \times 10^{-5}$ Hz, corresponding to a periodic displacement error of $\simeq 7$ mm at this frequency.) The raw frequency resolution of the spectrum is about 3×10^{-7} Hz. The spectrum in Figure 1 is smoothed to a resolution bandwidth of about 3×10^{-6} Hz to reduce estimation error. Approximate ± 2 σ confidence limits in the smoothed spectrum due to statistical estimation error only are indicated. Because the variance of a smoothed spectral estimator is approximately equal to the square of the true spectrum divided by the number of degrees of freedom used in its construction, the error bars will be the same across the spectrum on this log plot (Jenkins & Watts 1969).

The spectrum in Figure 1 consists of a continuum plus spectral lines between $\sim 10^{-5}$ and 10^{-4} Hz. The lines in the *un*smoothed spectrum are near the resolution limit of the 40 day observation; their apparent width in Figure 1 is due to the spectral smoothing. The lowest frequency line is near 1 cycle day^{-1}; the other lines are near harmonics of 1 cycle day^{-1}. Because of the multilink plasma correction, all random processes contributing to the spectrum of Figure 1 must be nondispersive. Below we construct upper limits to an isotropic GW background using this spectrum under the assumption that all the observed fluctuation power is due to GWs. To assess the conservatism of that assumption, we first discuss Doppler variability in the 10^{-6} to 10^{-2} Hz band and the extent to which it can be explained by known and independently determined noise processes.

3.1. *Doppler Noise Spectra for* $f > 10^{-4}$ Hz

At high frequencies ($f > 10^{-4}$ Hz) noise processes in the *Cassini*-era Doppler link have been well studied (Tinto 2002; Abbate et al. 2003). In this band the nondispersive continuum is dominated by a combination of thermal noise in the receiver, FTS noise, and a random process which has the correct level and temporal correlation for antenna mechanical noise. Figure 2 shows the temporal autocorrelation function of a representative DSS25 tracking pass during our observations. The data used to form this autocorrelation are from a two-way Ka-band track, after AMC calibration, and have dominant Fourier content in the band $\sim 10^{-4}$ to 10^{-1} Hz. From simultaneous differential X-Ka observations it is clear that Ka-band plasma scintillation at these Fourier frequencies contributes negligible fluctuation power. The positive correlation at the two-way light-time is characteristic of either mechanical noise in the ground tracking antenna, or a residual tropospheric process, and is reflected in Figure 1 as periodic modulation of the spectrum at high frequencies. From preexperiment verification of the AMC calibration process (Resch et al. 2002), the level of the observed autocorrelated noise is too high to be reasonably ascribed to tropospheric calibration error but is consistent with independent estimates of antenna mechanical noise in this band (Tinto 2002; Abbate et al. 2003). Positive correlation at T_2 is *not* consistent with the time series being dominated by a broadband isotropic GW background at high Fourier frequencies (Estabrook & Wahlquist 1975); thus we know that $S_{y2}^{\rm gw}(f) \ll S_{y2}(f)$ integrated over the band. At Fourier frequencies where the transfer function of the antenna mechanical noise is zero [odd multiples of $1/(2T_2)$], the observed spectral levels are in excellent agreement with expectation for FTS and receiver noises (Tinto 2002; Abbate et al. 2003). Thus even at these frequencies, where

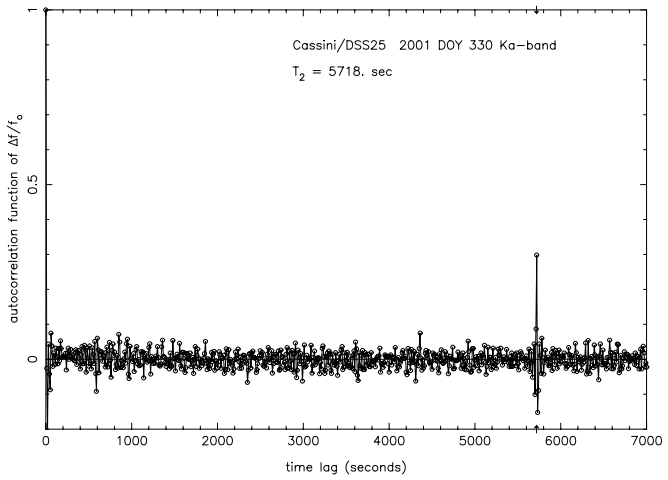

FIG. 2.—Representative temporal autocorrelation function of a tropospheric scintillation corrected Ka-band track, 2001 November 26, during the *Cassini* observations. Positive correlation at $\tau = T_2$ = two-way light-time is characteristic of all data taken during these observations. This temporal correlation structure is inconsistent with a broadband ($\simeq 10^{-4}$ to 10^{-2} Hz) GW background. See text.

our spectral densities are lowest, other nondispersive processes (including in principle GWs) cannot be a large fraction of the power.

3.2. *Doppler Noise Spectra for* $10^{-6}\,\mathrm{Hz} < f < 10^{-4}\,\mathrm{Hz}$

The low-frequency (10^{-6} to 10^{-4} Hz) Doppler error budget has not been as well studied. In this band, the observed S_{y2} is roughly an inverse power-law continuum plus spectral lines at geophysical frequencies. Obviously, any GW contribution to S_{y2} at 1 cycle day^{-1} and harmonics is small compared with the geophysical noise. The total variance of y_2 in this band is about 3×10^{-29} or, expressed as a rms path length variation on timescales $\simeq 10^4$–10^6 s, about 2 cm rms. In this region the instrument is operating in the LWL and low-frequency expansions of spectral transfer functions apply. The contributions to S_{y2} from the nondispersive noise processes frequency and timing system noise, noise due to spacecraft motion, spacecraft electronics noise, ground electronics noise, residual tropospheric noise after AMC calibration, and noise due to antenna mechanical motion are thus

$$S_{y2} \simeq 4\pi^2 T_2^2 f^2 S_y^{\mathrm{FTS}}(f) + S_y^{\mathrm{s/c\,motion}}(f) + S_y^{\mathrm{s/c\,elect.}} + S_y^{\mathrm{ground\,elect.}} + 4S_y^{\mathrm{tropo}}(f) + 4S_y^{\mathrm{ant}}(f)\ .$$

FTS noise is conventionally characterized in the time domain by the Allan deviation, $\sigma_y(\tau)$, the structure function of locally time-averaged fractional frequency fluctuations (Barnes et al. 1971). This is related to the two-sided spectrum of fractional frequency fluctuations: $\sigma_y^2(\tau) = \int_0^\infty 4S_y(f)\sin^4(\pi f\tau)/(\pi f\tau)^2 df$. Independently measured Allan deviations of hydrogen masers for $\tau = 10^5$–10^6 s give $\sigma_y \simeq 2 \times 10^{-15}(\tau/10^5\ \mathrm{s})^{1/2}$. The corresponding S_y^{FTS} is $\simeq 5 \times 10^{-36}(f/1\ \mathrm{Hz})^{-2}\ \mathrm{Hz}^{-1}$ for $\simeq 10^{-6}$ to 10^{-5} Hz. This spectrum is suppressed in the two-way Doppler by the LWL transfer function $4\pi^2 T_2^2 f^2$, giving $S_{y2}^{\mathrm{FTS}} \simeq 7 \times 10^{-27}\ \mathrm{Hz}^{-1}$ in the $\simeq 10^{-6}$ to 10^{-5} Hz band. FTS noise in S_{y2} is thus too small to contribute significantly in the low-frequency part of the spectrum.

Noise spectra of spacecraft motion, and electronics noise (spacecraft and ground) have not been independently studied in the 10^{-4} to 10^{-6} Hz band. Plausible extrapolations of spectra of these processes measured for $f > 10^{-4}$ Hz (Won & Lee 2001; Abbate et al. 2003) suggest that these processes contribute much less fluctuation power than is observed at low frequencies, however.

Spectra of uncalibrated water-vapor fluctuations on vertical tropospheric paths have been published for data taken in Denver, Colorado (Hogg et al. 1981). The tropospheric fluctuation power level they observed varied in order of magnitude, depending on tropospheric conditions. The one-dimensional phase spectrum they obtained was proportional to f^{-2} between 10^{-5} and 10^{-4} Hz (i.e., S_y^{tropo} independent of frequency in this band) with corresponding level $S_y^{\mathrm{tropo}} \simeq (1\text{–}10) \times 10^{-25}\ \mathrm{Hz}^{-1}$. The AMC calibrates $\simeq$90% of the rms variation; i.e., the corrected spectrum is expected to be about 1% of the uncorrected spectrum, so that $S_y \simeq (1\text{–}10) \times 10^{-27}\ \mathrm{Hz}^{-1}$. Accounting for the transfer function, the contribution to S_{y2} due to low-frequency calibrated troposphere, $4S_y^{\mathrm{tropo}}$, is $\simeq (4\text{–}40) \times 10^{-27}\ \mathrm{Hz}^{-1}$ in this decade band. This level is close to what is observed in Figure 1 near 10^{-4} Hz but substantially below the continuum level at lower frequencies. (A much more extensive unpublished data set of zenith tropospheric fluctuations taken at the Goldstone site [S. Keihm 2003, private communication] also gives spectra of calibrated wet component too small to be a major contributor to the low-frequency spectrum.) Thus the residual wet component, after calibration, probably contributes less than 10% of the observed low-frequency variance (and has a spectral shape different than is observed).

Antenna mechanical noise, a leading residual noise at higher Fourier frequencies, has not been directly measured in the 10^{-6} to 10^{-4} Hz band. At these low frequencies the aggregate antenna mechanical fluctuation effect is probably composed of approximately random processes (e.g., stochastic wind loading of the antenna, atmospheric pressure loading of the station, differential thermal expansion of the structure) and low-level quasi-deterministic processes (e.g., imperfections in the azimuth track the antenna rolls on, uncompensated gravity loading of the dish as the antenna's elevation angle changes, systematic errors in the subreflector focusing, etc.). Thermal processes (e.g., response of the structure to $\simeq$10 K temperature variations over a track) can, on a 34 m structure, plausibly produce several millimeters of path-length variation. The subreflector is continuously repositioned to approximately compensate for elevation-angle–dependent antenna distortions; systematic errors at the several millimeter level over the course of a track are not unreasonable. Additionally, there are systematic height variations in the azimuth track which will cause path-length variability. At DSS15 (another NASA/DSN antenna at Goldstone, having structural design similar to that of DSS25) height variations of the azimuth track are independently measured to be 6 mm peak to peak (DSS25 has not been independently measured). Systematic azimuth ring height variations and subreflector focusing errors, repeated over 40 days, are candidate contributors for at least the 1 cycle day^{-1} line. (For example, 6 mm path-length variations, smooth over horizon-to-horizon tracks and repeated daily in a 40 day observation, can give a $\sim 10^{-24}\ \mathrm{Hz}^{-1}$ spectral line at 1 cycle day^{-1}, comparable to what is observed.) Thus $\simeq$1 cm of low-frequency path variability due to aggregate unmodeled random and systematic motion within the ground antenna is expected. Additional time-dependent station displacements of $\simeq$1 cm due to atmospheric loading of the ground station (e.g., MacMillan & Gipson 1994; VanDam et al. 1994; Chen & Herring 1997) and other station position variations are expected also to contribute to Doppler noise at low frequency. Independently determined VLBI error budgets (minus components due to radio source structure, uncalibrated troposphere, and charged particle scintillation that are not in common with our observations) are believed to be dominated by station position and antenna mechanical noises and similarly account for $\simeq$1.3 cm rms path delay (Sovers, Fanselow, & Jacobs 1998).

Thus although the understanding of fluctuations at $f < 10^{-4}$ Hz is poorer than at higher frequencies, FTS noise, spacecraft motion noise, electronics noise (spacecraft and ground), and postcalibration residual tropospheric noise are probably *not* significant contributors. About one-half of the variance observed at low frequencies can be accounted for in terms of expected slow changes associated with the ground station (low-frequency antenna mechanical noise and atmospheric loading). This leaves about 1/2 of the variance in this band to other unknown mechanisms (including, in principle, GWs).

4. BOUNDS ON A STOCHASTIC BACKGROUND

The level of stochastic GWs is conventionally expressed in two ways: as the energy density in GWs relative to closure density or as a characteristic rms strain. For an isotropic GW spectrum, $S_h(f) = S_{y2}^{\rm gw}(f)/\bar{R}_2(f)$. For an isotropic background, the ratio of the energy density in GWs relative to the closure density, Ω, under the assumption that the energy density spectrum is locally flat and has bandwidth equal to center frequency, $f = f_c$, is (see the Appendices)

$$\Omega(f) = \frac{\pi f^3 S_{y2}^{\rm gw}(f)}{G\bar{R}_2(f)}\rho_{\rm crit}^{-1} = \frac{8\pi^2 f^3 S_{y2}^{\rm gw}(f)}{3\bar{R}_2(f)H_0^2}, \quad (5)$$

where $\rho_{\rm crit} = 3H_0^2/8\pi G$ is the closure density $\simeq 1.06 \times 10^{-29} h_{75}^2$ grams cm^{-3}, and h_{75} is the Hubble constant, H_0, in units of 75 km s^{-1} Mpc^{-1}. Alternatively, the bound on the background can be expressed as a characteristic strain amplitude (Thorne 1987; Rajagopal & Romani 1995; Jaffe & Backer 2003), $h_c(f) = [2fS_{y2}^{\rm gw}/\bar{R}_2(f)]^{1/2}$, where the factor of 2 arises because our spectra are two-sided.

To produce upper limits, we use the above equations, with $S_{y2}^{\rm gw}$ replaced with the observed total spectrum, S_{y2}:

$$\Omega(f) < \frac{8\pi^2 f^3 S_{y2}(f)}{3\bar{R}_2(f)H_0^2}, \quad (6)$$

$$h_c(f) < \left[\frac{2fS_{y2}}{\bar{R}_2(f)}\right]^{1/2}. \quad (7)$$

The above inequalities are obviously strictly true for ensemble average spectra: the statistical independence of the GW signal and the instrumental noises implies that $S_{y2}(f) > S_{y2}^{\rm gw}(f)$, since $S_{y2}^{\rm other}(f) > 0$ (eq. [4]). Of course we do not measure ensemble average spectra, but rather the smoothed spectrum of an individual realization of the *Cassini* Doppler and (in tests) smoothed spectra of individual realizations of the noises. In principle, due to fortuitous cancellation of Fourier components of the GW signal and the noises in a single realization, the resulting smoothed sample spectrum might not bound the ensemble average GW spectrum and the strict inequality above could be violated. However, the consistency of the observed spectrum with the aggregate noise spectrum places limits on possible violation of the inequalities.

The low- ($<10^{-4}$ Hz) and high-frequency ($>10^{-4}$ Hz) regions are considered separately. In the low-frequency part of the band there are $\simeq$33 independent smoothed spectral estimates. From § 3.2, about one-half of the total power is not accounted for by identified noise processes and thus could in principle be from GWs (obviously much less than one-half the power at the geophysical lines, 1 cycle day^{-1} and harmonics, however). Consider the case of equal power in signal and noise. Each smoothed spectral estimate in Figure 1 is the average of the squares of 11 complex numbers [Fourier transform of the $y_2(t)$ series, at full frequency resolution], each complex number being the vector sum of signal and noise. If there were equal ensemble average power in the signal and noise, the probability that a smoothed spectral estimate accidentally fluctuates down to be smaller than the ensemble average GW power, thus violating the inequality, is (by simulation) about 0.025. Thus fortuitous cancellation would, on average, lead to a violation of the strict inequality at fewer than one of the independent spectral estimates below 10^{-4} Hz.

In the high-frequency part of the band, the positive autocorrelation at T_2 implies that $S_{y2} \gg S_{y2}^{\rm gw}$, integrated over frequencies greater than about 10^{-4} Hz. The $\cos^2(\pi f T_2)$ transfer function of the principal noise, antenna mechanical fluctuations, causes minima in the total spectrum at odd multiples of $1/(2T_2)$. The excellent agreement of the spectrum at these frequencies with the power expected from secondary noises (FTS, receiver noise) indicates that S_{y2} has at most a small fraction of the power in processes not accounted for. Even if at every frequency there were ensemble average GW power with level 25% of the total power, the probability that a smoothed estimate of the total spectrum would fluctuate to below the ensemble average GW power is, by simulation, such that fewer than one of the $\simeq$3300 independent spectral estimates with $f > 10^{-4}$ Hz would be expected to violate the inequality. Because of the very small chance that *any* of the smoothed spectral estimates underestimates the ensemble average GW power, we present upper limits using the strict inequalities in equations (6) and (7).

Figure 3 expresses the upper limits in terms of Ω as a function of Fourier frequency using S_{y2} and equation (6), with H_0 = Hubble constant to be 75 km s^{-1} Mpc^{-1}. At 1.2×10^{-6} Hz, $\Omega < 0.025 \times h_{75}^{-2}$. Between 1.2×10^{-6} and $\simeq 10^{-5}$ Hz, $\Omega < 0.1 \times h_{75}^{-2}$, while between about 10^{-5} and 10^{-4} Hz the upper bounds are between 0.1 to about $1.0 \times h_{75}^{-2}$. For $f > 10^{-4}$Hz, our limits, expressed in terms of Ω, are larger than 1.

Figure 4 restates the limits from the spectrum of Figure 1 in terms of $h_c(f)$ (eq. [7]). Our lowest limits, $h_c < 2 \times 10^{-15}$, occur at about 0.3 mHz, set by the minimization of the antenna mechanical noise through its transfer function, the bandwidth, and the average coupling of the GW to the Doppler, $\bar{R}_2$, at this frequency.

Finally, the above expressed GW limits in the conventional ways (Ω and h_c). Alternatively, the results can be expressed directly as limits to the strain spectrum for an isotropic GW background: $S_h(f) = S_{y2}^{\rm gw}(f)/\bar{R}_2(f) < S_{y2}(f)/\bar{R}_2(f)$. This is done in Figure 5. At low frequencies,

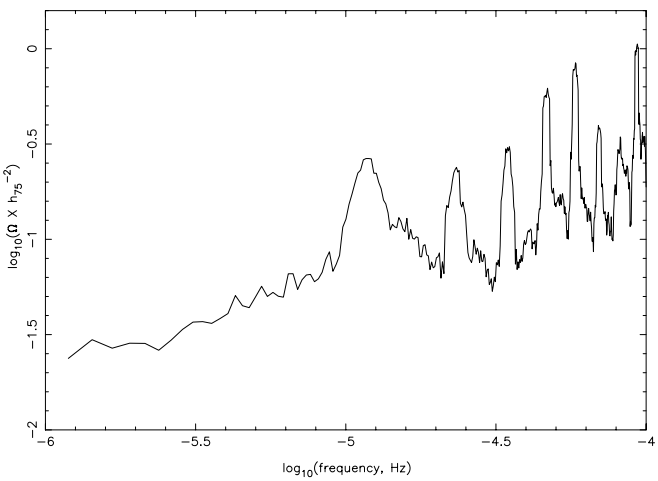

FIG. 3.—Upper limits to energy density of GWs in bandwidth equal to center frequency for an isotropic GW background, derived from the spectrum of Fig. 1, with $H_0 = 75$ km s^{-1} Mpc^{-1}.

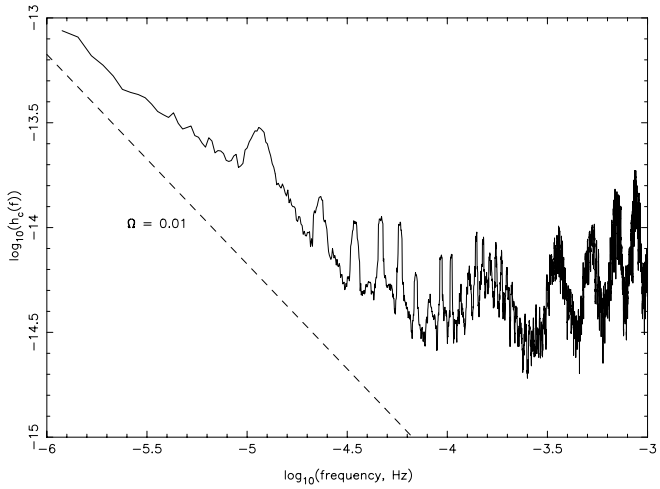

FIG. 4.—Upper limits from the spectrum of Fig. 1, restated in terms of characteristic strain $h_c(f) = [2fS_h(f)]^{1/2}$. Constant $\Omega = 0.01$ is indicated.

the suppression of the GW signal by the transfer function (eq. [2]) causes poorer upper bounds. At high frequencies, the GW coupling is good and S_{y2} is lower, resulting in improved upper limits. In particular at odd multiples of $1/(2T_2)$, the transfer function of antenna mechanical noise is zero and the best limits are set by the levels of secondary noises to be less than 6×10^{-27} Hz^{-1}.

5. DISCUSSION AND SUMMARY

A stochastic GW background can be either cosmological (if its origin is at the big bang) or astrophysical (if it is from an incoherent superposition of GWs from sources formed after the big bang). In order for a cosmological background to be consistent with the standard model of primordial nucleosynthesis, and its striking agreement with observations, the overall closure parameter for the present-day radiation content of the universe must be less than about 10^{-5}. Limits to Ω much smaller than 10^{-5} are achieved at nanohertz frequencies using pulsar timing (Detweiler 1979; Romani & Taylor 1983; Hellings & Downs 1983; Steinbring et al. 1990; Kaspi et al. 1994; Lommen 2001) and thus address both cosmological and astrophysical backgrounds at Fourier frequencies much lower than those considered in this paper. The $\sim 10^{-5}$ nucleosynthesis bound is below the sensitivity of spacecraft Doppler tracking in the 10^{-6} to 10^{-3} Hz band, however, so our data address only upper limits for an astrophysical background in the LF band.

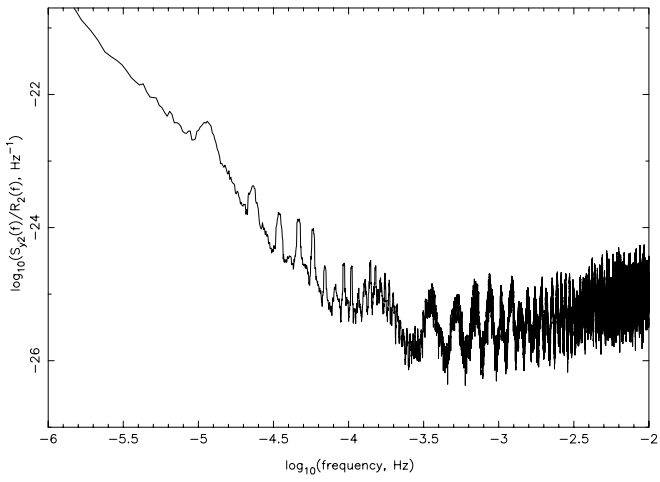

FIG. 5.—Upper limits to two-sided gravitational wave strain spectrum for an isotropic background: $S_h(f) < S_{y2}(f)/\bar{R}_2(f)$. The periodic modulation of the spectrum at high frequencies is due to the transfer function of antenna mechanical noise. Where this transfer function is zero—odd multiples of $1/(2T_2)$, where T_2 is the two-way light-time—our sensitivity is set by secondary noises and lowest upper limits are obtained.

Predictions for an astrophysical GW background in the 10^{-4} to 10^{-3} Hz band have been mainly aimed at future dedicated GW missions, e.g., LISA (Bender et al. 1998). Radiation from an ensemble of galactic binary stars will produce a GW background that will be important for LISA (Bender & Hils 1997) but is at a level too low for the *Cassini* detector. At somewhat lower frequencies (nanohertz–microhertz), an astrophysical GW background from an ensemble of coalescing black hole binaries is estimated to produce $h_c \sim 10^{-16}(f/1 \text{ cycle yr}^{-1})^{-2/3}$ (Rajagopal & Romani 1995; Jaffe & Backer 2003). Our lowest frequency, 10^{-6} Hz, barely overlaps the highest frequency of these model estimates. At 1 μHz, the models predict $h_c \sim 10^{-17}$, significantly below the observational limit that *Cassini* can impose (Fig. 4). Thus our limits, although the best observationally available at 1 μHz and higher, do not constrain current model predictions of an astrophysical background.

The spectral levels of fractional frequency fluctuations in Figure 1 are much lower than previously published spectra in this band. In addition to bounding a stochastic GW background, they illustrate the level of instrumental noise that can be achieved in radio observations on timescales of 10^2–10^6 s, relevant to the noise budgets of other radio science and radio astronomy observations. As an example of the latter, the spectrum of Figure 1 can be recast in terms of the spectrum of aggregate instrumental noises common to our observations and pulsar timing. The contribution to pulsar timing noise in the 10^{-6} to 10^{-4} Hz band due to path-length variation associated with the antenna with this system would be less than 100 ps.

We have measured the power spectrum of fractional frequency fluctuations in the two-way Doppler tracking of *Cassini* during its 2001–2002 solar opposition. Using the *Cassini* multilink radio system and the AMC, the effects of the formerly dominating noises—plasma and tropospheric scintillation—were, respectively, removed and calibrated to levels lower than other noises. The resulting data were used to construct upper limits to the strength of an isotropic GW background in the 10^{-6} to 10^{-3}Hz band. Our results are summarized in Figures 3, 4, and 5 as limits on energy density, characteristic strain, and spectrum of GW strain, respectively. The best limits are $\Omega < 0.025 \times h_{75}^{-2}$ at 1.2×10^{-6} Hz, $h_c < 2 \times 10^{-15}$ at about 0.3 mHz, and $S_h(f) < 6 \times 10^{-27}$ Hz^{-1} at odd multiples of $1/(2T_2)$. In the 10^{-6} to 10^{-4} Hz band the limits to Ω, for example, are $\simeq$500–1200 times better than previous Doppler determinations (Anderson & Mashhoon 1985). These limits are likely to remain the best direct observational bounds to a stochastic background in this band until a dedicated GW observatory in space, LISA, is flown about a decade from now.

The precision Doppler tracking capability described here is the result of dedicated work by many people. Crucial roles were played by colleagues at NASA, in the *Cassini* Project, the Deep Space Network, and the JPL Technical Divisions;

the contributions of these individuals are gratefully acknowledged. We especially thank our colleagues H. D. Wahlquist and F. B. Estabrook for long-time collaborations and fundamental contributions to low-frequency GW experiments. For J. W. A., the research described here was carried out at the Jet Propulsion Laboratory, California Institute of Technology, under a contract with the National Aeronautics and Space Administration. The work by L. I., P. T., and B. B. has been funded under ASI and MIUR contracts.

APPENDIX A

SPECTRAL COMPOSITION OF Ω

If a spectral energy density of gravitational waves (in units of the critical density $\rho_{\rm crit}$) $\tilde{\Omega}_{\rm gw}(f)$ is measured in a limited band around a frequency f_1, in the assumption that we have a wide-band process with bandwidth $\Delta f \approx f_1$, it is customary to estimate the total energy $\Omega_{\rm gw} = \int_0^\infty df \tilde{\Omega}_{\rm gw}(f)$ as $\Omega_{\rm gw}^{\rm obs} = f_1 \tilde{\Omega}_{\rm gw}(f_1)$. In gravitational wave experiments, for instance, this is what one does with resonant bar detectors, when the source is thought to be a catastrophic, wide-band collapse to a neutron star or a black hole. When, however, the source is unknown and we do not know whether the detection frequency f_1 has a physical significance, the quantity $\Omega_{\rm gw}^{\rm obs}$ energy sets only a *lower limit* to the total energy: not only an unknown amount of energy can reside at undetected frequencies $f \ll f_1$, but energy could also be present in a wide band at $f \gg f_1$, quite beyond the observed band. In our case we have a different problem: the observed spectral energy density $\tilde{\Omega}(f) > \tilde{\Omega}_{\rm gw}(f)$ is only an *upper limit* to the gravitational wave contribution $\tilde{\Omega}_{\rm gw}(f)$ and the previous argument is not sufficient to determine a lower limit to the total energy $\Omega_{\rm gw}$. What can one generally conclude about this quantity from *Cassini*'s experiments, aside from specific, and unavailable, models of a widespread collapse after nucleosynthesis?

The obvious limit $\Omega_{\rm gw} < \int_{f_1}^{f_2} df \tilde{\Omega}_{\rm gw}^{\rm obs}(f)$ is uninteresting, because the observed quantity $\tilde{\Omega}_{\rm gw}^{\rm obs}(f)$ increases at high frequency and, therefore, unless it can be subtracted away deterministically, the bound grows with f_2. Since a generated background has a wide-band spectrum, it is customary to use the dimensionless quantity

$$\Omega_{\rm gw}^{\rm obs} = f \tilde{\Omega}_{\rm gw}^{\rm obs}(f) \quad (f_1 < f_2)$$

to estimate $\Omega_{\rm gw}$. However, $\Omega_{\rm gw}$ may depend on the spectral shape decades of frequency away from the observed range (f_1, f_2); such extrapolation is meaningful if some assumption is made about the spectrum. The natural assumption—consistent with the origin of the background from a generalized collapse of a wide distribution of objects—is a power law $\tilde{\Omega}_{\rm gw}(f) = Kf^{-\alpha}$. There are three cases. If $\alpha > 1$, we need a low-frequency cutoff f_l and $\Omega_{\rm gw} < [1/(\alpha - 1)](f/f_l)^{\alpha - 1} \Omega_{\rm gw}^{\rm obs}$. If $\alpha < 1$, we need a high-frequency cutoff and $\Omega_{\rm gw} < [1/(1 - \alpha)](f_u/f)^{1-\alpha} \Omega_{\rm gw}^{\rm obs}$. In these cases one can obtain a bound on $\Omega_{\rm gw}$ only in the case in which the relevant cutoff is in, or near to, the observation band. In the important case $\alpha = 1$, the background is scale-free, $\Omega_{\rm gw} < \Omega_{\rm gw}^{\rm obs} \ln(f_u/f_l)$, and a direct limit is obtained.

APPENDIX B

DOPPLER SPECTRA, $h_c(f)$, AND Ω

The relationship between the Doppler spectrum and the density parameter has been discussed previously (Bertotti & Carr 1980; Bertotti et al. 1983; Anderson & Mashhoon 1985; Dobrowolny & Iess 1986; Giampieri & Vecchio 1995). Here we derive equation (5) and the relationship between the Doppler spectrum and the characteristic strain, $h_c(f)$.

Using a method developed for the theory of spacecraft Doppler tracking as a GW detector (Estabrook & Wahlquist 1975) and applying it to the pulsar case [a one-way measurement of Doppler from pulsar to Earth, in the limit $f \gg c/$(pulsar-Earth distance)], the variance of pulse time of arrival (TOA) ($\langle R^2 \rangle$) can be related to the energy density in GWs (ρ) in an octave band centered on f, assuming that the spectrum of energy density is flat in that band (Detweiler 1979, eq. [20]): $\langle R^2 \rangle = (208/243) G \rho \pi^{-3} f^{-4}$. These TOA fluctuations can be converted to one-way fractional Doppler using the derivative theorem for Fourier transforms: the spectrum of the TOA residuals $[S_R(f)]$ and the spectrum of the (one-way) fractional Doppler $[S_{y1}^{\rm gw}(f)]$ are related by $S_R(f) = S_{y1}^{\rm gw}(f)/(4\pi^2 f^2)$. The variance of the TOA residuals is twice the integral of S_R between $f_c/2$ and $3f_c/2$, where the factor of 2 arises because we use two-sided spectra throughout. By assumption, the spectrum of energy density is flat, thus the above results yield $\langle R^2 \rangle = (104/81) \pi^{-2} f^{-1} S_{y1}^{\rm gw}(f)$.

Detweiler's result is for the high-frequency limit in a one-way observation. By Fourier transforming, squaring, and averaging over the sky, one obtains the average one-way transfer function between $S_{y1}^{\rm gw}$ and $S_h(f)$. It is easy to show that, in the high-frequency limit, $S_{y1}^{\rm gw}(f) \rightarrow (2/3) S_h(f) = (2/3) S_{y2}(f)/\bar{R}_2(f)$.

Combining the above equations gives ρ in terms of the GW contribution to the two-sided, two-way fractional Doppler spectrum and the average three-pulse response function:

$$\rho = \frac{\pi f_c^3 S_{y2}^{\rm gw}(f_c)}{G \bar{R}_2(f_c)} \ . \tag{B1}$$

The ratio to the critical density, $\rho_{\rm crit} = 3H_0^2/8\pi G$, is Ω.

For comparison with other results we can rewrite this in terms of the variance of the fractional frequency fluctuations in an octave band: $\sigma^2 \simeq 2 f_c S_{y2}^{\rm gw}(f)$. In the LWL, $\bar{R}_2(f) \simeq (8/15)(\pi f T_2)^2$, so that the above equation for ρ becomes

$\rho_{\rm LWL} \simeq (15/16)\sigma^2/(G\pi T_2^2)$, in exact agreement with the result for Ω in the LWL computed independently by Giampieri & Vecchio (1995) (their eqs. [34] and [35]).

Alternatively, one can express the strength of the stochastic GW background in terms of the characteristic strain, $h_c(f)$, the square root of the product of the frequency, and the one-sided spectrum of strain at that frequency (Thorne 1987; Rajagopal & Romani 1995; Jaffe & Backer 2003). We obtain S_h from $S_{y2}^{\rm gw}$ and the sky-averaged transfer function $\bar{R}_2$: $h_c(f) = [2fS_{y2}^{\rm gw}(f)/\bar{R}_2(f)]^{1/2}$, where the factor of 2 arises because we use two-sided spectra.

REFERENCES

Abbate, S. F., et al. 2003, Proc. SPIE, 4856, 90
Anderson, J. D., & Mashhoon, B. 1985, ApJ, 290, 445
Armstrong, J. W., Estabrook, F. B., & Tinto, M. 1999, ApJ, 527, 814
Barnes, J. A., et al. 1971, IEEE Trans., IM-20, 105
Bender, P., Danzmann, K., & the LISA Study Team. 1998, Laser Interferometer Space Antenna for the Detection of Gravitational Waves (Pre-Phase A Rep., MPQ233; Garching: Max-Planck-Institüt für Quantenoptik)
Bender, P. L., & Hils, D. 1997, Classical Quantum Gravity, 14, 1439
Bertotti, B., & Carr, B. J. 1980, ApJ, 236, 1000
Bertotti, B., Carr, B. J., & Rees, M. J. 1983, MNRAS, 203, 945
Chen, G., & Herring, T. A. 1997, J. Geophys. Res.–Solid Earth, 102, 20489
Detweiler, S. 1979, ApJ, 234, 1100
Dobrowolny, M., & Iess, L. 1986, A&A, 157, 346
Estabrook, F. B., Tinto, M., & Armstrong, J. W. 2000, Phys. Rev. D, 62, 042002
Estabrook, F. B., & Wahlquist, H. D. 1975, General Relativ. Gravitation, 6, 439
Giampieri, G., & Vecchio, A. 1995, General Relativ. Gravitation, 27, 793
Hellings, R. W., & Downs, G. S. 1983, ApJ, 265, L39
Hogg, D. C., Guiraund, F. O., & Sweezy, W. B. 1981, Science, 213, 1112
Iess, L., et al. 1999, Classical Quantum Gravity, 16, 1487
———. 2003, in Proc. IEEE Aerospace Conference, 2003 March 8-15, Big Sky, Montana (Piscataway: IEEE)
Jaffe, A. H., & Backer, D. C. 2003, ApJ, 583, 616
Jenkins, G. M., & Watts, D. G. 1969, Spectral Analysis and Its Applications (San Francisco: Holden Day)
Kaspi, V. M., Taylor, J. H., & Ryba, M. F. 1994, ApJ, 428, 713
Kliore, A. J., et al. 2003, Space Sci. Rev., in press
Lommen, A. N. 2001, Ph.D. thesis, Univ. California
MacMillan, D. S., & Gipson, J. M. 1994, J. Geophys. Res.–Solid Earth, 99, 18081
Rajagopal, M., & Romani, R. W. 1995, ApJ, 446, 543
Resch, G. M., et al. 2002, IPN Prog. Rep., 42-148, 1
Romani, R. W., & Taylor, J. H. 1983, ApJ, 265, L35
Sovers, O. J., Fanselow, J. L., & Jacobs, C. J. 1998, Rev. Mod. Phys. 70, 1393
Steinbring, D. R., Ryba, M. F., Taylor, J. H., & Romani, R. W. 1990, Phys. Rev. Lett., 65, 285
Tanner, A. B., & Riley, A. L. 2003, Radio Science, 38, 8050
Thorne, K. S. 1987, in Three Hundred Years of Gravitation, ed. S. Hawking & W. Israel (Cambridge: Cambridge Univ. Press), 330
Tinto, M. 2002, Classical Quantum Gravity, 19, 1767
Tortora, P., Iess, L., & Ekelund, J. E. 2002, in Proc. World Space Congress, 2002 October 10–19, Houston (Houston: IAF/COSPAR)
Tortora, P., Iess, L., & Herrera, R. G. 2003, in Proc. IEEE Aerospace Conference, 2003 March 8–15, Big Sky, Montana (Piscataway: IEEE)
VanDam, T. M, Blewitt, G., & Heflin, M. B. 1994, J. Geophys. Res.–Solid Earth, 99, 22939
Wahlquist, H. D. 1987, General Relativ. Gravitation, 19, 1101
Wahlquist, H. D., Anderson, J. D., Estabrook, F. B., & Thorne, K. S. 1977, Atti dei Convengni Lincei, 34, 335
Won, L., & Lee, A. 2001, JPL Internal Memo. SCO-01-044 (Pasadena: JPL)